



COMMUNICATION

Manganese oxide nanoparticles supported on graphene oxide as an efficient nanocatalyst for the synthesis of 1,2,4-oxadiazoles from aldehydes

Fariba Saadati^{1,2} | Babak Kaboudin³ | Rana Hasanloei¹ |
Zeinab Namazifar¹ | Xavier Marset⁴ | Gabriela Guillena³

¹Department of Chemistry, Faculty of Science, University of Zanjan, Zanjan, 45371-38791, Iran

²Department of Chemistry, University of British Columbia, 2036 Main Mall, Vancouver, British Columbia, V6T 1Z1, Canada

³Department of Chemistry, Institute for Advanced Studies in Basic Sciences (IASBS), Gava Zang, Zanjan, 45137-66731, Iran

⁴Departamento de Química Orgánica, e Instituto de Síntesis Orgánica (ISO), Universidad de Alicante, Alicante, 03080-Alicante, Spain

Correspondence

Fariba Saadati, Department of Chemistry, Faculty of Science, University of Zanjan, Zanjan 45371-38791, Iran; Department of Chemistry, University of British Columbia, 2036 Main Mall, Vancouver, British Columbia V6T 1Z1, Canada.
Email: saadati@znu.ac.ir; fsaadati@chem.ubc.ca

The easy synthesis of graphene oxide (GO)-supported manganese dioxide (MnO₂) nanoparticles as a stable heterogeneous nanocatalyst (MnO₂@GO) is described. This catalyst was investigated in the synthesis of 1,2,4-oxadiazoles from amidoximes and aldehydes via a cyclization and oxidation process. The nanocomposite was prepared and characterized using various techniques. The catalytic application of the nanocomposite was examined in the reaction of a variety of aldehydes with aliphatic and aromatic amidoximes. The stable and robust catalyst was recycled for seven consecutive runs without a significant decrease in the catalytic activity.

KEYWORDS

1,2,4-oxadiazole, graphene oxide, manganese dioxide, nanoparticles, oxidation

1 | INTRODUCTION

The synthesis of heteroaromatic ring systems has been widely researched, owing to their presence in a multitude of biologically and medicinally active compounds. Among these heteroaromatic rings, substituted 1,2,4-oxadiazoles have a myriad of applications in bioactive molecules and pharmacophore scaffolds like muscarinic receptors,^[1] serotonergic antagonists,^[2] growth hormone secretagogues^[3] and inhibitors of human neutrophil elastase^[4] and tyrosine kinase.^[5] Furthermore, some 1,2,4-oxadiazole derivatives are of interest as anti-inflammatory,^[6] antirhinoviral,^[7] antibacterial^[8] and anticancer agents.^[9,10] In addition, they have also been employed as bioisosteres for esters and

amides in peptide mimetics,^[11] ligands for transition metal complexes^[12] and liquid crystals.^[13]

Several methods have been developed for the synthesis of 1,2,4-oxadiazole derivatives as reported in the literature. 1,3-Dipolar cycloaddition of nitrile oxides with nitriles^[14] and azetine^[15] has been reported. The most popular strategy for the synthesis of 1,2,4-oxadiazoles is the *O*-acylation of amidoximes using activated carboxylic acid derivatives such as benzoyl cyanides,^[16] esters,^[17,18] anhydrides,^[19,20] acid chlorides^[21,22] and carboxylic acids,^[23] followed by intramolecular cyclodehydration. Another method for the synthesis of 1,2,4-oxadiazole derivatives is the reaction of amidoxime with aldehydes for the synthesis of 4,5-dihydro-1,2,4-oxadiazoles, followed by oxidative dehydrogenation

with chemical oxidants^[24,25] or electrochemical oxidation methods.^[26] However, several drawbacks are associated with these methods.^[27] Toxicity and instability of acid chlorides make them hard to handle and store. Oxidants are required in stoichiometric amounts relative to the substrate. Therefore, the development of more efficient, simple, economical and environmentally benign methodologies is still needed for the synthesis of substituted 1,2,4-oxadiazoles.

Recently, heterogeneous catalysts containing nanoparticles have been applied to chemical reactions as an effective strategy to address the claims of green chemistry.^[28] In this context, the chemistry of manganese is extremely rich because of its easily accessible Mn(II), Mn(IV) and Mn(VII) oxidation states^[29] and its natural abundance.^[30] In comparison with other manganese species, manganese oxide nanoparticles have great potential for applications in adsorption of hazardous dyes,^[31,32] imaging contrast agents,^[33] super capacitors^[34,35] and a new generation of catalysts^[36,37] due to their high surface area, electrochemical activity, natural abundance, environmentally benign nature and low cost. However, the small particle size as well as the high surface area of nanoparticles makes them thermodynamically susceptible to agglomeration processes, leading to the formation of larger inactive particles. A valuable approach to overcome this problem is the development of ecofriendly and biodegradable solid materials as supports.^[38] Along this line, various solid supports including cellulose,^[39] biochar,^[40] graphene^[41] and reduced graphene oxide^[42,43] have been reported as supports for MnO₂ nanoparticles. Graphene oxide (GO) is a single sheet of graphite oxide with excellent mechanical properties, high surface area and desirable compatibility with materials, which make it a promising substrate in material chemistry and catalysis.^[44]

To the best of our knowledge, there has been no previous study of the synthesis of 1,2,4-oxadiazoles from aldehydes in the presence of heterogeneous catalyst. As part of our continuing investigation of the preparation, characterization and application of nanocatalysts,^[45,46] herein we report the preparation and characterization of MnO₂ nanoparticles supported on GO sheets (MnO₂@GO). The catalytic performance of the new material was studied in the synthesis of 3,5-disubstituted 1,2,4-oxadiazole derivatives from the reaction of amidoximes with aldehydes.

2 | EXPERIMENTAL

2.1 | Materials

The chemicals and solvents were purchased from commercial suppliers and used without further purification.

TLC analysis was performed using Merck silica gel 60F254 analytical plates to follow the progress of reactions. Purification was done using column chromatography on Merck silica gel 60 (*n*-hexane–ethyl acetate as eluent). Deionized water was used for washing and solution preparation.

2.2 | Apparatus and instrumentation

Fourier transform infrared (FT-IR) spectra were recorded using a Bruker Vector 22 FT-IR spectrophotometer with KBr/Nujol mull in the range 400–4000 cm⁻¹ under ambient conditions. ¹H NMR and ¹³C NMR spectra were recorded with a Bruker spectrometer, at frequencies of 250 and 62.5 MHz, respectively, in CDCl₃. X-ray diffraction (XRD) patterns were collected with Bruker D8-Advance with Göebel mirror X-ray diffractometer using Cu-K α radiation ($\lambda = 1.54 \text{ \AA}$). Thermogravimetric analysis (TGA) and differential scanning calorimetry (DCS) were performed with a DSC/TG thermal analyzer (Netzsch STA 409 PC/PG) using Al₂O₃ pans under air atmosphere from ambient temperature to 800°C with a heating rate of 5°C min⁻¹. The morphology and elemental composition of synthesized products were studied using a MIRA3TESCAN-XMU field emission scanning electron microscopy (FE-SEM) instrument and energy-dispersive X-ray analysis (EDX). An NT-MDT NTEGRA PRIMA atomic force microscopy (AFM) instrument was utilized to investigate the surface topography and height profile of samples in air by depositing a drop of a dilute suspension on a clean mica surface. Tapping mode cantilevers (NT-MDT NSG-01) had force constants of 1.45–15.1 N m⁻¹, resonant frequencies between 87 and 230 kHz and a tip curvature radius of 6 nm. The chemical composition of products was investigated using X-ray photoelectron spectroscopy (XPS) with a fully automated K-Alpha spectrometer (Thermo-Scientific). Flame atomic absorption spectrophotometry (AAS; Varian Spectra AA 220 FS) was used for the determination of the level of metal ions. All pH measurements were done with a Metrohm pH meter (model 780) equipped with a combined glass electrode. An M-UV-3⁺ Zolalan (Iran) water purification system was utilized to produce deionized water.

2.3 | Methods

2.3.1 | Preparation of MnO₂@GO nanocatalyst

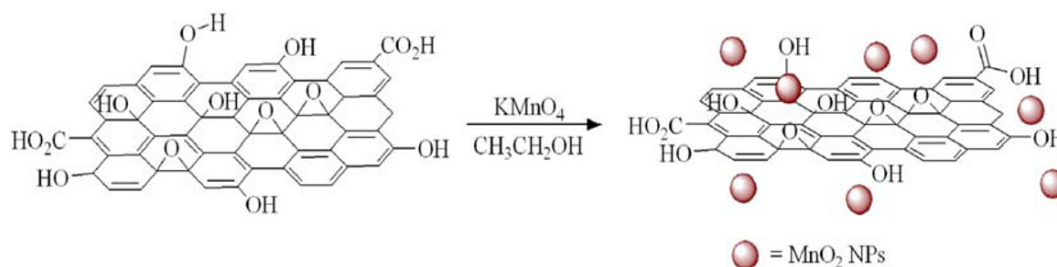
GO was prepared by acid oxidation according to a modified Hummers method.^[47] A mixture of graphite powder

(1.5 g) and sodium nitrate (1.5 g) in sulfuric acid (70 ml) was stirred in an ice bath for 20 min. After that, potassium permanganate (9 g) was introduced into the mixture and the temperature was kept at 40°C and stirred for 30 min. To this solution, 100 ml of deionized water was gradually added. The exothermic reaction resulted in an increase of the solution temperature to 98°C. At this stage deionized water (300 ml) and H₂O₂ (10 ml) were slowly added to the reaction mixture. Afterwards the resulting solid material was washed with 100 ml of diluted hydrochloric acid (0.1 M). The mixture was centrifuged and the supernatant was decanted away. The remaining mixture was then washed successively with water until the pH value of the solution was 4. Finally, the prepared GO was centrifuged and dried under vacuum.

The resultant GO (0.3 g) was dispersed in ethanol (8 ml) and deionized water (5 ml) by sonicating for 2 h. An aqueous solution of potassium permanganate (0.032 g in 2 ml) was added dropwise. The mixed solution was then stirred at 35°C for 6 h. Finally, the mixture was centrifuged, washed with water and ethanol to remove the remaining residual and dried in an oven at 60°C.

2.3.2 | General procedure for synthesis of 3,5-disubstituted 1,2,4-oxadiazoles

MnO₂@GO (0.14 g, 4 mol%) was dispersed in 1,4-dioxane (1.5 ml) for 10 min. Amidoxime (1 mmol) and aldehyde (1.5 mmol) were added and the reaction mixture was refluxed for 24 h. The reaction progress was monitored by TLC. After the reaction was finished, the mixture was washed with methanol (4 × 2 ml) and centrifuged. The combined organic extracts were dried over MgSO₄, and concentrated *in vacuo*, and the corresponding product was afforded by column chromatography on silica gel 60 (*n*-hexane–ethyl acetate) in high yield. The characterization data resulting from ¹H NMR and ¹³C NMR spectroscopy and elemental analyses are provided in Data S1.



SCHEME 1 MnO₂@GO preparation procedure

3 | RESULTS AND DISCUSSION

GO as solid support was easily prepared through oxidation of graphite with acid-KMnO₄ via a modified Hummers method.^[47,48] The resulting functionalized GO was then used to support MnO₂ nanoparticles which were easily prepared in the presence of KMnO₄ and ethanol (Scheme 1). The application of the functionalized GO plays a significant role in the reduction of Mn⁷⁺ to Mn⁴⁺ by the presence of carbon atoms and anchoring KMnO₄ and then MnO₂ onto GO sheets due to their high hydrophilicity.

It is also interesting to note that the strong interactions of GO through its functional groups with MnO₂ nanoparticles may prevent the agglomeration and produce a more durable and robust heterogeneous catalyst.

Manganese loading on the MnO₂@GO was determined using AAS analysis to be 0.28 mmol g⁻¹.

The FT-IR spectra of the GO and MnO₂@GO nanocomposite were investigated in order to get detailed information about the chemical functional moieties present in the material (Figure 1). Figure 1a shows the FT-IR spectrum of the prepared GO. All characteristic peaks at approximately 3400, 1733, 1600,

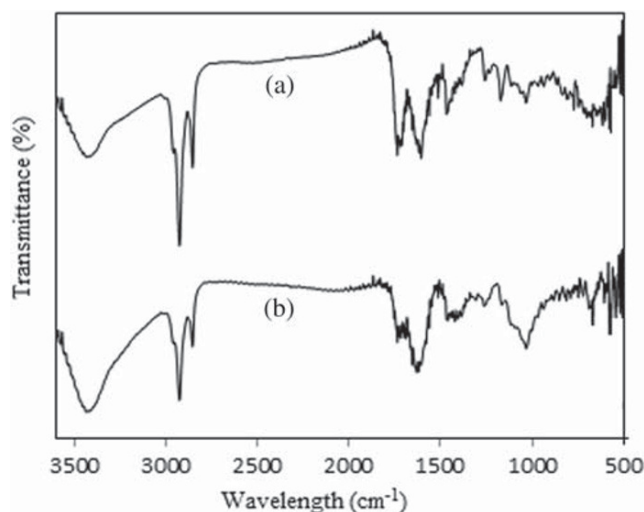


FIGURE 1 FT-IR spectra of (a) GO and (b) MnO₂@GO

1240 and 1025 cm^{-1} can be assigned to OH, C=O, C=C, carbonyl C=O and epoxy C=O, respectively. The peaks at 2920 and 2850 cm^{-1} are due to the vibrations of $=\text{CH}_3$ and $=\text{CH}_2$, respectively. Comparison of the FT-IR spectra shows that all the bands of GO remained in the $\text{MnO}_2@\text{GO}$ spectrum (Figure 1b). The absorption band at about 560 cm^{-1} is attributed to the Mn=O stretching vibration while that at 1220 cm^{-1} is attributed to the stretching of hydrated MnO_2 .^[49]

Raman spectra of GO and $\text{MnO}_2@\text{GO}$ were recorded (Figure 2). As can be seen, there are no significant differences between them. Both spectra present D and G peaks centered at *ca* 1343 and *ca* 1590 cm^{-1} , respectively, a broad 2D peak at around 2670 cm^{-1} and a second-order band centered at *ca* 2850 cm^{-1} .^[50]

TGA and differential thermoanalysis (DTA) were applied for investigation of the thermal behavior of the prepared $\text{MnO}_2@\text{GO}$ nanocomposite. The TGA curve of sample can be mainly divided into four consecutive weight losses between 25 and 800 °C (Figure 3). The first weight loss, about 10.49% below 115 °C, is attributed to

desorption of chemisorbed and physisorbed water and organic solvents. A large weight loss at around 115–310 °C (27.13%) corresponded to the release of CO, CO₂ and steam due to the decomposition of the oxygen functional groups of the GO layers. The next mass loss occurred at around 310–570 °C with a weight loss of 18.94%, presumably due to the combustion of the carbon skeleton of the nanocomposite. The last weight loss, occurring at about 570 °C, is due to the release of lattice oxygen from the decomposition of MnO_2 into Mn_2O_3 .^[36] The gradual weight loss during the analysis confirms the thermal stability of the prepared nanocatalyst.

The DSC technique was applied for the investigation of the thermal behavior of the prepared nanocomposite. The DSC profile reveals two exothermic events at around 209 and 401 °C with caloric value of -608 and -114.2 J g^{-1} for $\text{MnO}_2@\text{GO}$ (Figure 4).

Figure 5 shows the XRD patterns of GO and $\text{MnO}_2@\text{GO}$. The diffraction peak at 2θ of around 12.25° can be ascribed to the (001) plane of GO nanosheets. On the basis of this peak, the interlayer spacing is larger than

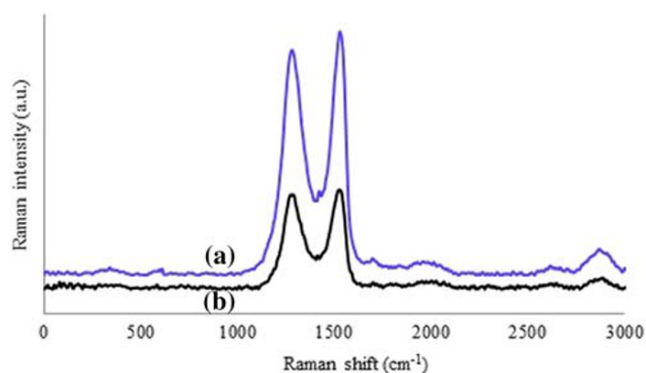


FIGURE 2 Raman spectra of (a) GO and (b) $\text{MnO}_2@\text{GO}$

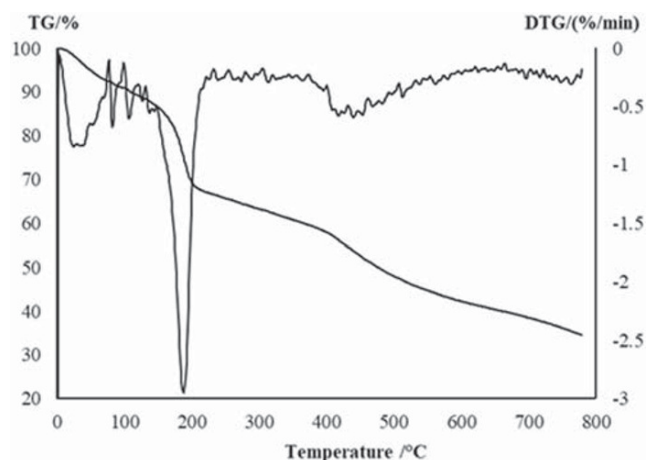


FIGURE 3 Thermogravimetric diagram of $\text{MnO}_2@\text{GO}$

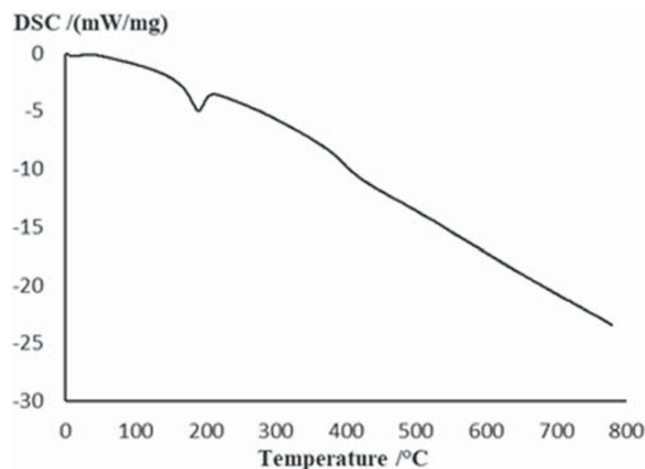


FIGURE 4 DSC analysis of $\text{MnO}_2@\text{GO}$

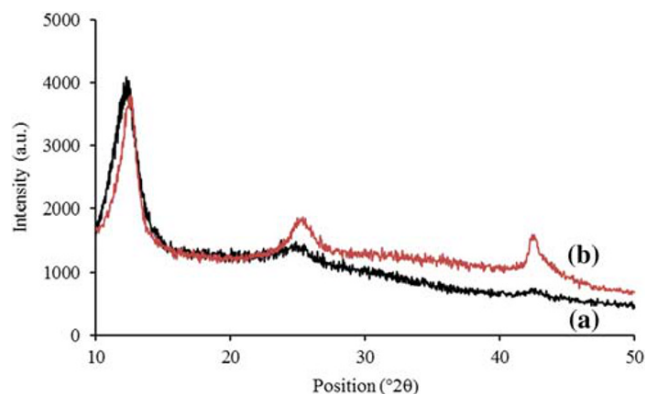


FIGURE 5 XRD patterns of (a) GO and (b) $\text{MnO}_2@\text{GO}$

in graphite due to the introduction of oxygen-containing functional groups on the graphite sheets. The XRD pattern of the $\text{MnO}_2@\text{GO}$ is similar to that observed for pure GO.

Furthermore, from the EDX data (Figure 6), C, O and Mn are the main elements of $\text{MnO}_2@\text{GO}$. Apparently, C was the most abundant constituent in the composite which comes from the support backbone. The EDX results indicated that MnO_2 had been successfully incorporated in the nanocomposite.

FE-SEM analysis was employed to visualize the morphology of the nanocatalyst (Figure 7). The FE-SEM images of GO and $\text{MnO}_2@\text{GO}$ with wrinkles and folds clearly indicated a two-dimensional planar and

multilayer structure of the support. The results also reveal that MnO_2 nanospheres are densely dispersed on the surface of GO sheets owing to chemical interactions (Figure 7b).

The detailed elemental composition of the as-prepared $\text{MnO}_2@\text{GO}$ nanocomposite was probed using XPS and the corresponding results are presented in Figure 8. According to the Mn 2p spectrum, two strong peaks of Mn 2p_{3/2} and Mn 2p_{1/2} were centered at 642.38 and 653.58 eV, respectively (Figure 8a).^[51] This result implies that Mn^{7+} was successfully reduced to Mn^{4+} on the surface of the GO. XPS analysis further confirmed the presence of carbon and functional groups in GO by showing the peaks related to C 1s at 284.68, 285.68, 287.58 and

FIGURE 6 EDX analysis of $\text{MnO}_2@\text{GO}$

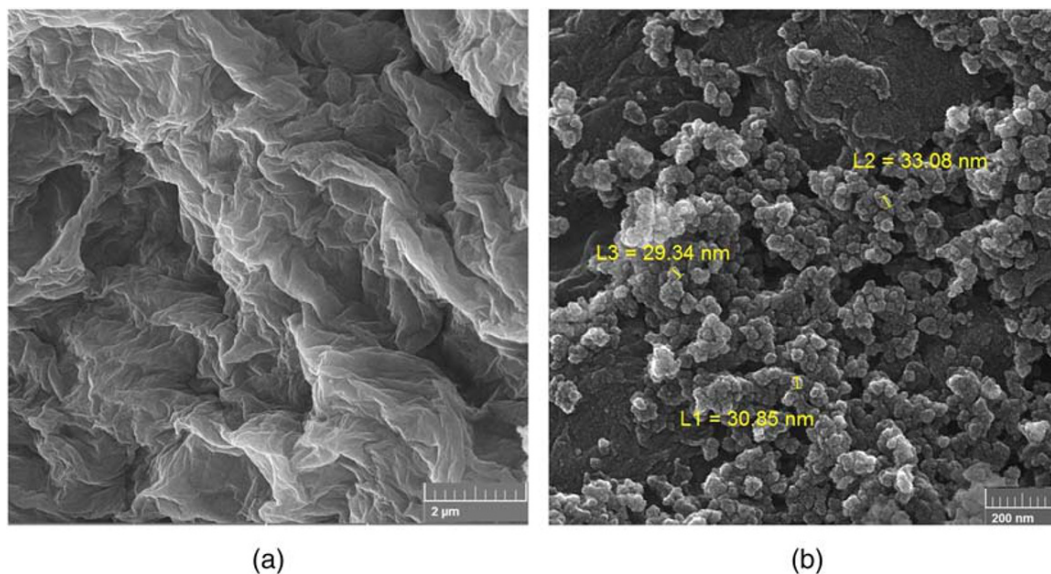
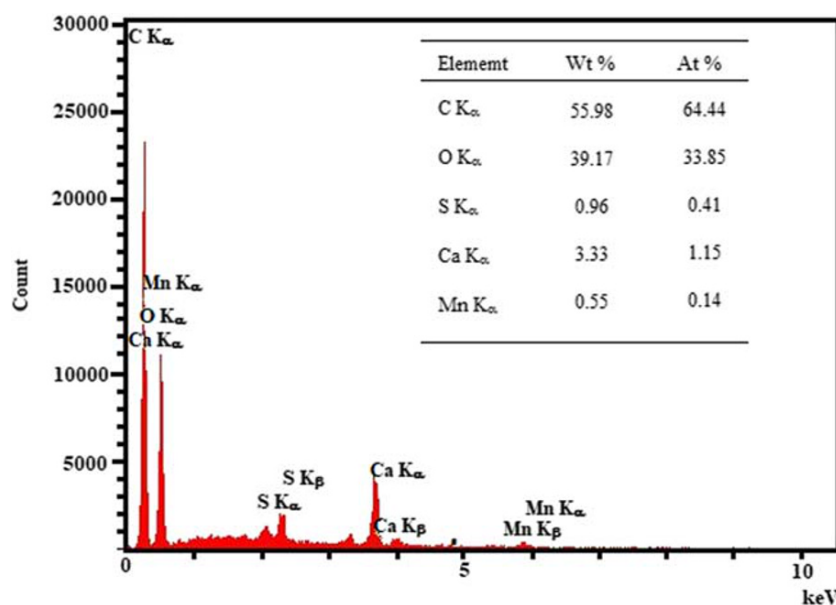


FIGURE 7 FE-SEM images (a) GO and (b) $\text{MnO}_2@\text{GO}$

289.28 eV corresponding to C=C/C=C, C=O, C=O and O=C=O, respectively (Figure 8b).^[52]

Surface topography was observed for nanoparticles on the GO surface using AFM. Figure 9 shows the two- and three-dimensional AFM images of nanocomposite dispersion in water after deposition on a freshly cleaved mica surface. The AFM image reveals that the MnO₂ particles are spherical as deposited on the GO sheets.

A histogram of particle size distribution obtained from AFM measurements for MnO₂ particles is shown in Figure 10. Statistical analysis confirmed an average diameter of 24 nm.

To further understand the catalytic performance of the MnO₂@GO nanocatalyst, a comprehensive study of the synthesis of 1,2,4-oxadiazoles from aldehydes was carried out. In order to determine the optimal reaction

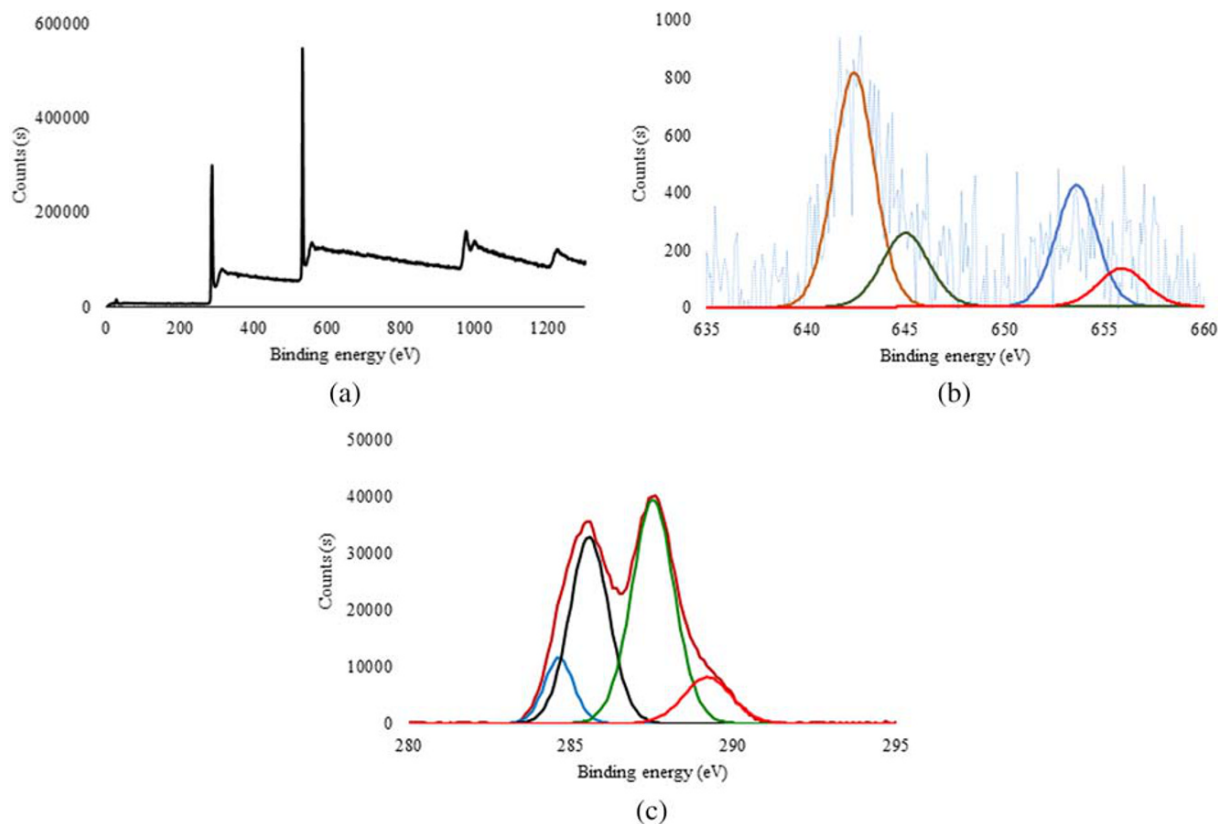


FIGURE 8 XPS spectra of MnO₂@GO: (a) full range and (b) Mn 2p and (c) C 1s regions

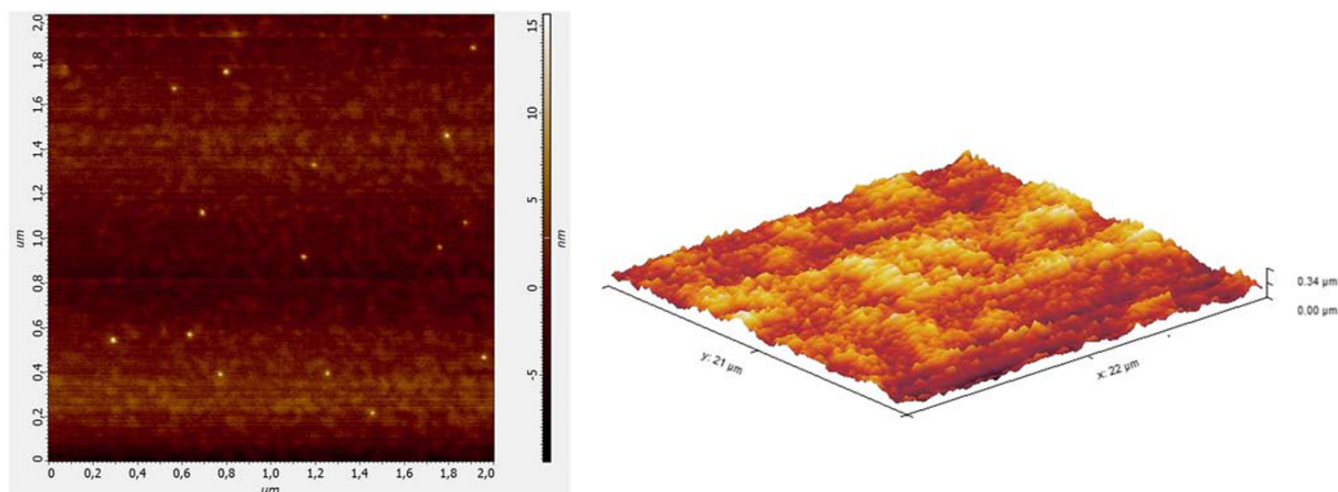


FIGURE 9 Two- and three-dimensional AFM images of MnO₂@GO composite

conditions, the coupling of benzaldehyde with benzamidoxime was investigated as a model reaction in the presence of the nanocatalyst (Table 1). In this reaction, various amounts of catalyst were surveyed and it was found that lower amounts of MnO_2 decreased the reaction yield (Table 1, entries 1–3). To further determine the solvent effect, the reaction was carried out in solvents

other than 1,4-dioxane, such as CHCl_3 , CH_3CN , water, ethanol and toluene. Moderate yields were obtained when the reaction was performed in ethanol and acetonitrile, and no product was generated in CHCl_3 , water and toluene under the same reaction conditions (Table 1, entries 3–8). Also, it was found that increasing the reaction temperature to 95°C improved the reaction efficiency

FIGURE 10 Particle size distribution histogram for $\text{MnO}_2@\text{GO}$

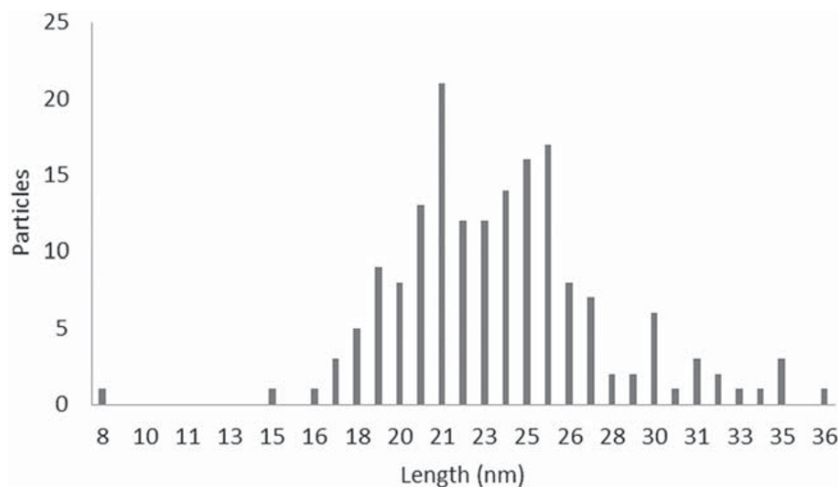
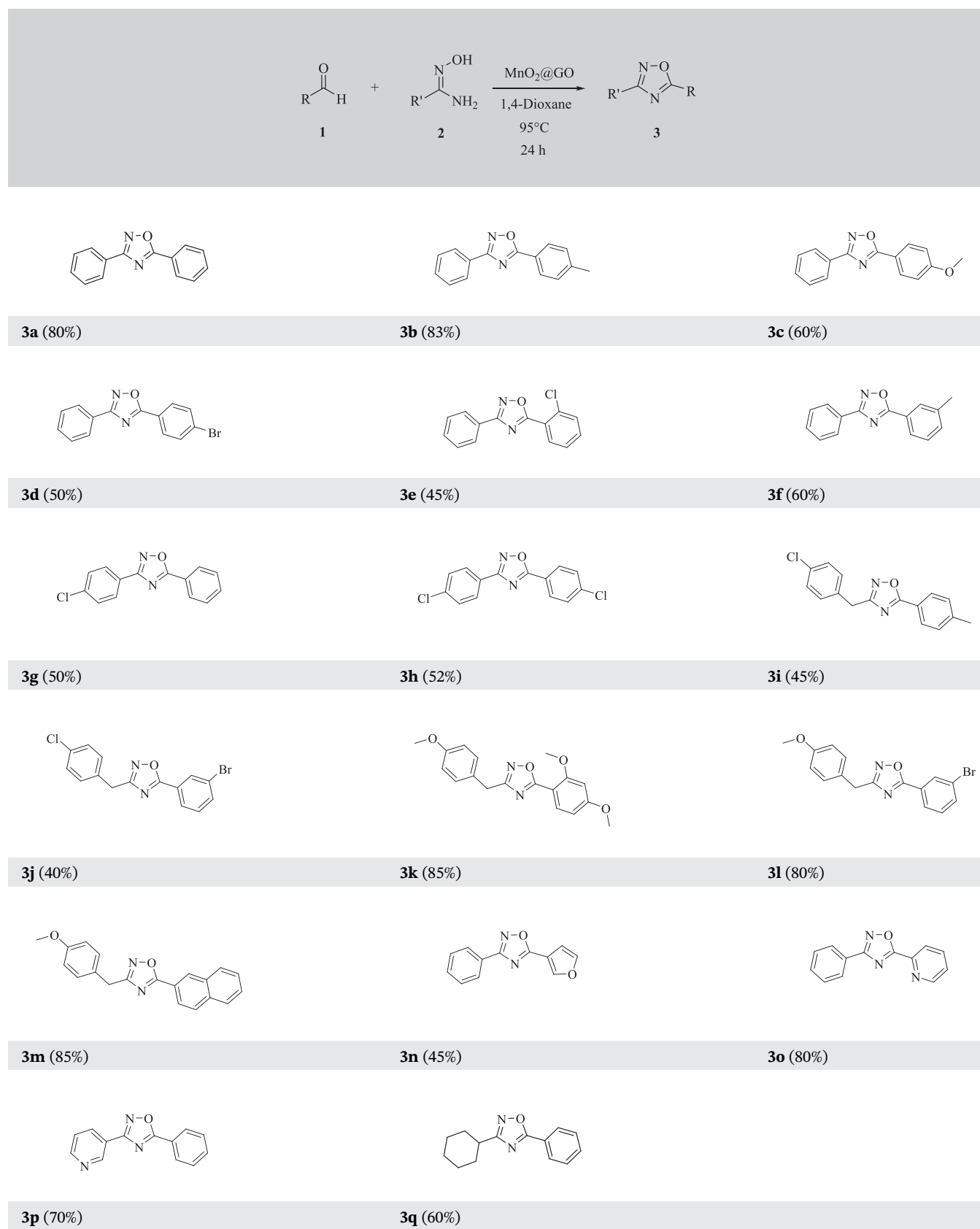


TABLE 1 Screening of various parameters for reaction of benzamidoxime and benzaldehyde^a

Entry	Catalyst (mol %)	Solvent	Temp. ($^\circ\text{C}$)	Time (h)	Yield (%) ^b
1	2	1,4-Dioxane	95	24	28
2	3	1,4-Dioxane	95	24	75
3	4	1,4-Dioxane	95	24	80
4	4	CHCl_3	60	24	—
5	4	H_2O	100	24	—
6	4	Toluene	100	24	—
7	4	EtOH	78	24	25
8	4	CH_3CN	80	24	55
9	4	1,4-Dioxane	80	24	45
10	4	1,4-Dioxane	50	24	15
11	4	1,4-Dioxane	30	24	5
12	4	1,4-Dioxane	95	12	40
13	4	1,4-Dioxane	95	6	24
14	-	1,4-Dioxane	95	24	20

^aReaction conditions: benzamidoxime (1 mmol), benzaldehyde (1.5 mmol), catalyst (X mol%) and solvent (1.5 ml).

^bIsolated yield.

TABLE 2 Synthesis of 1,2,4-oxadiazoles by reaction of aldehydes with amidoximes in the presence of MnO₂@GO nanocatalyst^a

^aReaction conditions: amidoxime (1.0 mmol), aldehyde (1.5 mmol), catalyst (4 mol%) and solvent (1.5 ml).

SCHEME 2 Proposed mechanism for formation of 1,2,4-oxadiazoles using $\text{MnO}_2@\text{GO}$ nanocatalyst

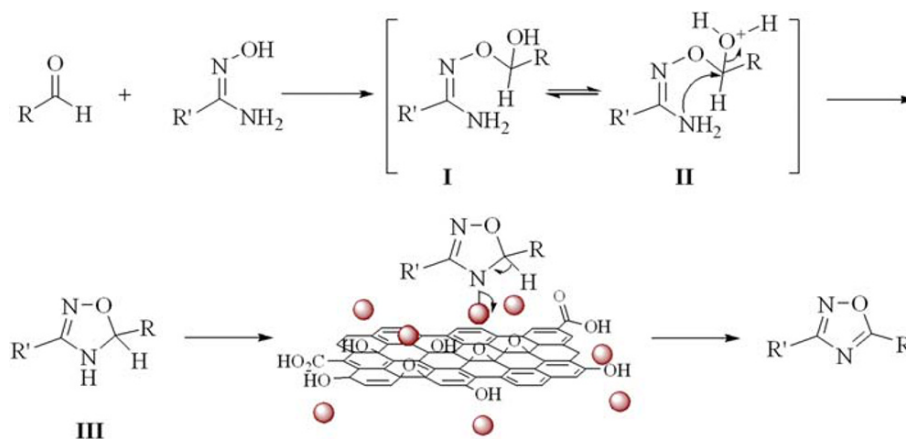


(Table 1, entries 9–11). Also, it was found that only 24 and 40% of the desired product was obtained after 6 and 12 h (Table 1, entries 12 and 13).

Having established the optimal reaction conditions, the scope and limitations of the reaction were next examined in the presence of 4 mol% nanocatalyst in 1,4-dioxane for various types of amidoximes and aldehydes at 95°C (Table 2).

In this survey, aromatic aldehydes with electron-donating groups reacted very quickly, while in the case of using aldehydes with electron-withdrawing groups, the reactivity decreased and longer reaction times were required (Table 2). It is important to mention that sterically congested *ortho*-substituted benzaldehyde gave the corresponding product in moderate yield (Table 2, **3e**). To broaden the utility of the nanocatalyst the reaction was investigated with heteroaromatic aldehydes and amidoxime and the results showed that they reacted successfully to furnish the corresponding oxadiazoles (Table 2, **3n–p**). Furthermore, to extend the scope of the reaction, various aliphatic and aromatic amidoximes were used, showing a good tolerance (Table 2, **3i–m** and **3q**). The results strongly confirm the capability of the $\text{MnO}_2@\text{GO}$ nanocatalyst in cyclization of a broad range of aldehydes with both aromatic and aliphatic amidoxime substrates.

The probable reaction mechanism for the synthesis of 1,2,4-oxadiazoles catalyzed by GO-supported MnO_2 nanoparticles under heterogeneous conditions is shown in Scheme 2. The reaction presumably occurs through nucleophilic addition of =OH functional group of amidoxime on the carbonyl function of aldehyde to form hemiacetal I, which is protonated under the reaction conditions (II).^[53] Then, intramolecular nucleophilic attack of the amino group to the protonated hemiacetal moiety provides 4,5-dihydro-1,2,4-oxadiazole (III). 3,5-Disubstituted 1,2,4-oxadiazole is obtained by oxidation of cyclic intermediate III.

Further, the leaching of manganese oxide from the catalyst was analyzed. The amount of manganese in the

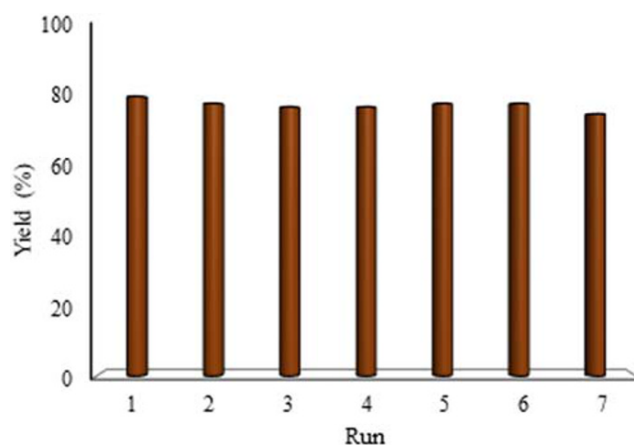


FIGURE 11 Recycling experiment of $\text{MnO}_2@\text{GO}$

recycled catalyst was determined from AAS analysis of the supernatant. In this regard, no significant leaching of manganese occurred during the reaction, indicating that the catalyst worked in a heterogeneous manner.

Therefore the recoverability and reusability of $\text{MnO}_2@\text{GO}$ was investigated in the reaction of benzamidoxime and benzaldehyde. After each reaction, the catalyst was separated from the reaction mixture by centrifugation and then was washed with methanol to remove organic materials and subsequently dried at 60°C. The recovered catalyst could be reused directly in further reactions. It was shown that the recovery can be effectively achieved for more than seven reaction runs without significant loss in product yields (Figure 11).

4 | CONCLUSIONS

A new manganese-based nanocomposite catalyst of MnO_2 nanoparticles on GO sheets was prepared and completely characterized. The developed material appears to be an efficient heterogeneous catalyst in the synthesis of 1,2,4-oxadiazoles from the reaction of

amidoximes with aldehydes via cyclization and oxidation process with broad scope of the substrates. Most importantly, the catalyst could be easily recycled and reused without significant loss of catalytic activity. The easy recovery, excellent performance and negligible leaching of metal species (none detected using AAS) mean that this protocol fulfills the criteria established for green catalysis. Such a suitable catalytic efficiency could be attributed to the high surface area, uniform distribution and favorable accessibility of the active sites in the prepared nanocatalyst.

ACKNOWLEDGEMENTS

The authors are grateful to the Research Council of University of Zanjan, Institute for Advanced Studies in Basic Sciences (IASBS), the University of British Columbia, the University of Alicante (VIGROB-173) and the Spanish Ministerio de Economía, Industria y Competitividad (CTQ2015-66624-P) for support of this work.

ORCID

Fariba Saadati  <https://orcid.org/0000-0002-7853-9503>

REFERENCES

- [1] J. E. Macor, T. Ordway, R. L. Smith, P. R. Verhoest, R. A. Mack, *J. Org. Chem.* **1996**, *61*, 3228.
- [2] C. Swain, R. Baker, C. Kneen, J. Moseley, J. Saunders, E. Seward, G. Stevenson, M. Beer, J. Stanton, K. Watling, *J. Med. Chem.* **1991**, *34*, 140.
- [3] M. Ankersen, B. Peschke, B. S. Hansen, T. K. Hansen, *Bioorg. Med. Chem. Lett.* **1997**, *7*, 1293.
- [4] K. Ohmoto, T. Yamamoto, T. Horiuchi, H. Imanishi, Y. Odagaki, K. Kawabata, T. Sekioka, Y. Hirota, S. Matsuoka, H. Nakai, *J. Med. Chem.* **2000**, *43*, 4927.
- [5] J. L. Buchanan, C. B. Vu, T. J. Merry, E. G. Corpuz, S. G. Pradeepan, U. N. Mani, M. Yang, H. R. Plake, V. M. Varkhedkar, B. A. Lynch, *Bioorg. Med. Chem. Lett.* **1999**, *9*, 2359.
- [6] R. M. Srivastava, A. de Almeida Lima, O. S. Viana, M. J. da Costa Silva, M. T. Catanho, J. O. F. de Morais, *Biorg. Med. Chem.* **2003**, *11*, 1821.
- [7] G. D. Diana, D. L. Volkots, T. J. Nitz, T. R. Bailey, M. A. Long, N. Vescio, S. Aldous, D. C. Pevear, F. J. Dutko, *J. Med. Chem.* **1994**, *37*, 2421.
- [8] N. Tka, B. Ben Hassine, *Synth. Commun.* **2010**, *40*, 3168.
- [9] A. Chimirri, S. Grasso, A. Monforte, A. Rao, M. Zappala, *Farmaco (Societa Chimica Italiana: 1989)* **1996**, *51*, 125.
- [10] H.-Z. Zhang, S. Kasibhatla, J. Kuemmerle, W. Kemnitzer, K. Ollis-Mason, L. Qiu, C. Crogan-Grundy, B. Tseng, J. Drewe, S. X. Cai, *J. Med. Chem.* **2005**, *48*, 5215.
- [11] S. Borg, R. C. Vollinga, M. Labarre, K. Payza, L. Terenius, K. Luthman, *J. Med. Chem.* **1999**, *42*, 4331.
- [12] A. Terenzi, G. Barone, A. P. Piccionello, G. Giorgi, A. Guarcello, A. Pace, *Inorg. Chim. Acta* **2011**, *373*, 62.
- [13] G. Q. Ali, I. H. R. Tomi, *Liq. Cryst.* **2018**, *45*, 421.
- [14] N. A. Bokach, A. V. Khripoun, V. Y. Kukushkin, M. Haukka, A. J. Pombeiro, *Inorg. Chem.* **2003**, *42*, 896.
- [15] K. Hemming, M. N. Khan, P. A. O'Gorman, A. Pitard, *Tetrahedron* **2013**, *69*, 1279.
- [16] S. Kandre, P. R. Bhagat, R. Sharma, A. Gupte, *Tetrahedron Lett.* **2013**, *54*, 3526.
- [17] S. Baykov, T. Sharonova, A. Shetnev, S. Rozhkov, S. Kalinin, A. V. Smirnov, *Tetrahedron* **2017**, *73*, 945.
- [18] K. K. Amarasinghe, M. B. Maier, A. Srivastava, J. L. Gray, *Tetrahedron Lett.* **2006**, *47*, 3629.
- [19] M. Tarasenko, N. Duderin, T. Sharonova, S. Baykov, A. Shetnev, A. V. Smirnov, *Tetrahedron Lett.* **2017**, *58*, 3672.
- [20] B. Kaboudin, L. Malekzadeh, *Tetrahedron Lett.* **2011**, *52*, 6424.
- [21] B. Kaboudin, F. Saadati, *Tetrahedron Lett.* **2007**, *48*, 2829.
- [22] B. Kaboudin, F. Saadati, *J. Heterocyclic Chem.* **2005**, *42*, 699.
- [23] R. F. Poulain, A. L. Tartar, B. T. P. Déprez, *Tetrahedron Lett.* **2001**, *42*, 1495.
- [24] D. N. Nicolaidis, K. C. Fylaktakidou, K. E. Litinas, D. Hadjipavlou-Litina, *Eur. J. Med. Chem.* **1998**, *33*, 715.
- [25] W. Wang, H. Xu, Y. Xu, T. Ding, W. Zhang, Y. Ren, H. Chang, *Org. Biomol. Chem.* **2016**, *14*, 9814.
- [26] M. Okimoto, Y. Takahashi, *Bull. Chem. Soc. Jpn* **2003**, *76*, 427.
- [27] A. R. Katritzky, A. A. Shestopalov, K. Suzuki, *ARKIVOC* **2005**, *7*, 36.
- [28] F. Shirini, M. Abedini, *J. Nanosci. Nanotechnol.* **2013**, *13*, 4838.
- [29] D. Kolb, *J. Chem. Educ.* **1988**, *65*, 1004.
- [30] S.-B. Ma, K.-W. Nam, W.-S. Yoon, X.-Q. Yang, K.-Y. Ahn, K.-H. Oh, K.-B. Kim, *J. Power Sources* **2008**, *178*, 483.
- [31] B. P. Kumar, K. Shivaprasad, R. Raveendra, R. H. Krishna, S. Karikkat, B. Nagabhushana, *Int. J. Appl. Innov. Eng. Manag.* **2014**, *3*, 102.
- [32] B. Kumar, S. Karikkat, R. H. Krishnac, T. Udayashankarab, K. Shivaprasada, B. Nagabhushanac, *Res. Rev. J. Mater. Sci.* **2014**, *2*, 27.
- [33] H. B. Na, J. H. Lee, K. An, Y. I. Park, M. Park, I. S. Lee, D. H. Nam, S. T. Kim, S. H. Kim, S. W. Kim, *Angew. Chem.* **2007**, *119*, 5493.
- [34] G. Zhao, J. Li, L. Jiang, H. Dong, X. Wang, W. Hu, *Chem. Sci.* **2012**, *3*, 433.
- [35] S. Chen, J. Zhu, X. Wu, Q. Han, X. Wang, *ACS Nano* **2010**, *4*, 2822.
- [36] K. Selvakumar, S. M. Senthil Kumar, R. Thangamuthu, K. Ganesan, P. Murugan, P. Rajput, S. N. Jha, D. Bhattacharyya, *J. Phys. Chem. C* **2015**, *119*, 6604.
- [37] L. Lu, H. Tian, J. He, Q. Yang, *J. Phys. Chem. C* **2016**, *120*, 23660.
- [38] B. R. Cuenya, *Thin Solid Films* **2010**, *518*, 3127.
- [39] S. M. Maliyekkal, K. P. Lisha, T. Pradeep, *J. Hazard. Mater.* **2010**, *181*, 986.
- [40] L. Zhou, Y. Huang, W. Qiu, Z. Sun, Z. Liu, Z. Song, *Molecules* **2017**, *22*, 173.
- [41] J. Chang, M. Jin, F. Yao, T. H. Kim, V. T. Le, H. Yue, F. Gunes, B. Li, A. Ghosh, S. Xie, *Adv. Funct. Mater.* **2013**, *23*, 5074.
- [42] M. Ramesh, M. P. Rao, F. Rossignol, H. Nagaraja, *Water Sci. Technol.* **2017**, *76*, 1652.
- [43] M. Kim, Y. Hwang, J. Kim, *J. Power Sources* **2013**, *239*, 225.
- [44] H. Wang, Q. Hao, X. Yang, L. Lu, X. Wang, *ACS Appl. Mater. Interfaces* **2010**, *2*, 821.

- [45] F. Saadati, N. Khani, M. Rahmani, F. Piri, *Catal. Commun.* **2016**, *79*, 26.
- [46] M. Gholinejad, F. Saadati, S. Shaybanizadeh, B. Pullithadathil, *RSC Adv.* **2016**, *6*, 4983.
- [47] W. S. Hummers Jr., R. E. Offeman, *J. Am. Chem. Soc.* **1958**, *80*, 1339.
- [48] F. Saadati, F. Ghahramani, H. Shayani-jam, F. Piri, M. R. Yaftian, *J. Taiwan Inst. Chem. Eng.* **2018**, *86*, 213.
- [49] M. Ananth, S. Pethkar, K. Dakshinamurthi, *J. Power Sources* **1998**, *75*, 278.
- [50] S. Claramunt, A. Varea, D. López-Díaz, M. M. Velázquez, A. Cornet, A. Cirera, *J. Phys. Chem. C* **2015**, *119*, 10123.
- [51] L. Peng, X. Peng, B. Liu, C. Wu, Y. Xie, G. Yu, *Nano Lett.* **2013**, *13*, 2151.
- [52] Z. Wang, Y. Dong, H. Li, Z. Zhao, H. B. Wu, C. Hao, S. Liu, J. Qiu, X. W. D. Lou, *Nat. Commun.* **2014**, *5*, 5002.
- [53] R. M. Srivastava, M. V. Freire, A. Chaves, T. M. Beltrão, G. B. Carpenter, *J. Heterocyclic Chem.* **1987**, *24*, 101.

SUPPORTING INFORMATION

Additional supporting information may be found online in the Supporting Information section at the end of this article.

How to cite this article: Saadati F, Kaboudin B, Hasanloei R, Namazifar Z, Marset X, Guillena G. Manganese oxide nanoparticles supported on graphene oxide as an efficient nanocatalyst for the synthesis of 1,2,4-oxadiazoles from aldehydes. *Appl Organomet Chem.* 2020;e5838. <https://doi.org/10.1002/aoc.5838>